USING A ONE-DIMENSIONAL SPRAY MODEL TO IMPROVE LIQUID LENGTH AND IGNITION DELAY ESTIMATIONS FOR DIESEL FLAMES

R. Payri, F. J. Salvador, J. De la Morena (*), V. Pagano

CMT-Motores Térmicos, Universitat Politècnica de València

Camino de Vera s/n, E-46022 Spain.

(*) Corresponding author:

Dr. Joaquin De la Morena, joadela@mot.upv.es

CMT-Motores Térmicos, Universitat Politècnica de València

Camino de Vera s/n, E-46022 Spain.

Telephone: +34-963877650

FAX: +34-963877659

ABSTRACT

In the current paper, a methodology based on the combination of a one-dimensional spray model and experimental correlations has been proposed to predict the physical time associated with ignition delay in diesel diffusion flames. This physical time depends significantly on the nozzle geometry, and its influence is not captured in traditional Arrhenius-like correlation. To assess this influence, three multi-hole nozzles with different degrees of conicity (expressed in terms of k-factor) have been tested on an optically accessible 2-stroke single-cylinder engine. First, the hydraulic behavior of the nozzles is assessed from the point of view of injection rate and spray momentum. Later, the effect of the geometry on vapor spray angle has been analyzed through a Schlieren visualization technique. Mie-scattering has allowed to determine the stabilized liquid length. Then, chemiluminescence imaging was used to obtain the temporal and spatial appearance of OH- radicals, which are used as indicators to the ignition delay. Finally, all the results are combined with a one-dimensional spray model to determine the physical induction time and include it into a new ignition delay correlation, which shows up to 4% accuracy improvement compared to a traditional Arrhenius equation.

KEY WORDS:

NOMENCLATURE

A	Constant in the ignition delay correlation
A_{eff}	Effective outlet area of a nozzle orifice
a,b	Coefficients for liquid length correlation
$C(x,r)$	Local fuel concentration at a given axial and radial position
C_a	Area coefficient
C_{axis}	Axial spray fuel concentration
C_{mv}	Fuel mass concentration needed in the spray axis to get complete evaporation
cns	Constant for LL correlation
C_v	Velocity coefficient
D_{eff}	Effective outlet diameter of a nozzle orifice.
D_i	Inlet diameter
D_o	Outlet diameter
E_A	Activation energy
ET	Energizing time
f	Radial velocity distribution function
i	Counter for numerical series into spray 1D model
K	Constant used in the ignition delay correlation.
$k\text{-}factor$	Nozzle conicity. Defined as $kfactor = 100 \cdot \dfrac{D_i - D_o}{L}$
k_s	Spray constant in LL analysis
L	Nozzle orifice length
LL	Liquid Length
$n\text{-}m$	Coefficients used in the ignition delay correlation.
$\dot{M}_o$	Spray momentum at the nozzle outlet

3

$\dot{M}(x)$	Spray momentum at a given axial position
$\dot{m}_o$	Mass flow at the nozzle outlet
P_{back}	Backpressure.
P_{inj}	Injection pressure.
r	Radial position inside the spray
R_u	Spray radius at an axial position x
R	Gas constant
ROI	Rate of Injection
Sc	Schmidt number
SMD	Sauter Mean Diameter of fuel droplets
SOI	Start of Injection
t_{mv}	Time for a fuel parcel in the axis of a stationary spray to reach a concentration equal to $C_{mv.}$
T	Temperature in the engine combustion chamber.
TDC	Top Dead Center
$U(x,r)$	Local spray velocity at a given axial and radial position
U_{axis}	Axial spray velocity
U_{eff}	Effective velocity at the outlet orifice, defined as $u_{eff} = C_a^{1/2} \cdot D_o$
x	Axial position inside the spray

Greek symbols:

α	Shape parameter for Gaussian radial velocity profile
ΔP	Pressure drop, $\Delta P = P_{inj} - P_{back.}$
$\rho(x,r)$	Local density inside the spray at a given axial and radial position.

ρ_a Ambient density.

ρ_f Liquid fuel density.

λ Wavelength

θ_m Spray angle defined from the fuel mass concentration Gaussian profile

θ_u Spray angle defined from the velocity Gaussian profile

τ Time elapsed from the start of the injection to start of combustion (ignition delay).

$\tau_{accuracy}$ Accuracy coefficient for the ignition delay correlations

τ_{exp} Experimental ignition delay

τ_{ini} Ignition delay estimated from initial correlation (w/o t_{mv})

τ_{new} Ignition delay estimated from new correlation (w/ t_{mv})

1. INTRODUCTION

The need for continuous emissions reduction has driven the optimization of internal combustion engines over the last decades [1]. In particular, in the case of diesel engines, special attention has been made to the design characteristics of the fuel injection system, due to its particular importance for spray formation and fuel-air mixing characteristics [2]–[6]. In this sense, Ning et al. [7] evaluated the effect of the nozzle orifices geometry on the hydraulic behavior of the injector, as well as the spray penetration. Yao et al. [8] studied the importance of the outlet diameter and length of the nozzle orifices on spray atomization, showing that the Sauter Mean Diameter (SMD) tends to decrease when lowering the diameter. Brusiani et al. [9] studied the effect of the nozzle orifices conity in the formation of cavitation inside the nozzle. Payri et al. [10] assessed that this cavitation formation can enhance spray atomization and fuel-air mixing performance close to the nozzle exit. Conicity and hydrogrinding have also shown to severely impact the flame lift-off length [11] and the overall spray and combustion processes [12][13].

In order to evaluate such aspects, different numerical methodologies have been developed to study the fuel injection processes along the last decades. One-dimensional multi-physical models have shown a good capability to predict the dynamic behavior of the injector and predict the instantaneous mass flow rate [14]–[16]. In the same way, one-dimensional spray models based on the gas jet analogy allow to obtain reasonable results in terms of spray penetration [17], [18] and global equivalence ratio distribution [19], once the hydraulic characteristics of the nozzle are known. Nevertheless, these simplified models cannot be used to study the fluid-dynamic details of the fuel injection system processes. For this reason, full three-dimensional CFD models have also been used to study the internal nozzle flow characteristics [20]–[22], the primary atomization processes [23], [24] and the overall spray features [4], [25].

One of the most important parameters to characterize diesel spray combustion is the ignition delay [26][27][28]. In diesel flames, the ignition delay is a result of the interaction between the physical processes (atomization, mixing and evaporation of the fuel spray) and chemical processes (pre-reaction kinetic rates). Several authors have seen over the years that the ignition delay can be predicted through an Arrhenius correlation based on the thermodynamic conditions (pressure, temperature and overall equivalence ratio) in the combustion chamber [29], [30]. Nevertheless, such correlations do not take into account the physical processes previously mentioned, which can be very relevant in the case of diesel applications. This is the reason why Pischinger et al. [31] introduced also the injection pressure as a way to account of its effect on fuel-air mixing. Kim et al. [5] showed that the physical properties of the fuel (mostly specific heat, density and viscosity) also impact the ignition delay. Finally, Payri et al. [32] developed a correlation of the ignition delay based on Arrhenius terms, but corrected to account for the nozzle outlet effective diameter and conicity.

In the current paper, a methodology based on the use of a spray model has been proposed as a means to estimate the physical time related to the diesel spray mixing and vaporization. In particular, a one-dimensional spray model, previously developed by the authors, has been used to estimate this physical time since it can capture the overall spray characteristics at a much lower computational cost compared to a full 3D-CFD simulation. This time will be later introduced into an Arrhenius correlation for the ignition delay, in order to decouple the physical and chemical processes into the diesel autoignition phenomena. For this purpose, three multi-hole nozzles with different level of conicity (k-factor), which have different spray characteristics, have been used. The main parameters needed to estimate the physical delay are the spray momentum, the effective outlet velocity, the spray angle and the stabilized liquid length. These

parameters will be experimentally obtained by means of the nozzles hydraulic characterization (mass flow rate and momentum flux) and spray visualization techniques for the vapor (Schlieren) and liquid (Mie-scattering) phases. The global ignition delay will be obtained from OH- chemiluminescence data.

The paper is divided in 7 sections. First, the different experimental arrangements used along the study are described in section 2. Then, the main equations existing on the one-dimensional spray model used for the study are defined in section 3. Section 4 details the results obtained from the hydraulic and spray combustion characterization. Section 5 is devoted to the estimation of the physical delay by combining the previous experimental data with the 1D modelling approach, while section 6 evaluates two different ignition delay correlations. Finally, the main conclusions of the study are drawn in section 7.

2. EXPERIMENTAL TOOLS

The complete experimental campaign has been carried out using a standard common-rail system and a European diesel fuel, which meets EN590 standard requirements. The main properties of the fuel are summarized in Table 1. It has to be highlighted that the fuel selected affects the particular values of liquid length and ignition delay, limiting the applicability of the correlations proposed in sections 5 and 6 to this particular fuel. Nevertheless, the methodology proposed could be applied to different fuels in future works.

2.1 Nozzles

Three multi-hole nozzles are used along the study. All of them are defined with the same Bosch flow number (stationary volumetric flow at $P_{inj} = 10$ MPa and $P_{back} = 0.1$ MPa), but different levels of conicity defined in terms of k-factor (2.0, 1.6 and 0 for

nozzles N1, N2 and N3, respectively). The inlet diameter of the orifices is approximately equal (175 µm), resulting in different levels of outlet diameters (155, 160 and 175 µm, respectively)

2.2   <u>Hydraulic characterization</u>

In order to provide the right boundary conditions to the spray model, the hydraulic performance of the nozzles has been assessed. First, a Rate Of Injection (ROI) meter based on the Bosch methodology [33] has allowed to obtain the instantaneous flow through the nozzle orifices. Using this facility, the fuel is injected in a pressurized tube filled with fuel. The injected fuel induces an increase of the pressure inside this tube, which is captured by a piezoelectric pressure transducer. This pressure signal is then post-processed to obtain the instantaneous mass flow rate, using the procedure described in [34].

Additionally, the momentum flux at the nozzle outlet is also measured with a custom-made test rig. In this case, the fuel is injected into a chamber filled with a pressurized inert gas (for example N_2), simulating engine-like densities. The momentum of the spray is assessed by measuring its impact force on a target placed perpendicular to a single nozzle orifice at a distance of approximately 5 mm from the exit. More details of the test rig and the methodology can be found in [35].

The test matrix used for both the injection rate and the momentum flux measurements are detailed in Table 2.A. As it can be seen, only relatively long injections have been characterized, since the objective is to obtain the flow coefficients at maximum needle lifts, where the flow is nearly steady state. At these conditions, the injection rate and momentum flux are no longer a function of the needle position, but depend only on the nozzle geometry and the fuel injector boundary conditions. For this

reason, all hydraulic results presented in the current paper will correspond to a time average of the injection rate and the momentum flux profiles on the quasi-steady state phase. Combining these values of mass flow and momentum flux, it is possible to define effective outlet velocity and diameter of the nozzle:

$$U_{eff} = \frac{\dot{M}_o}{\dot{m}_o} \tag{1}$$

$$\dot{m}_o = \rho_f A_{eff} U_{eff} = \rho_f \frac{\pi D_{eff}^2}{4} U_{eff} \tag{2}$$

$$D_{eff} = \sqrt{\frac{4\dot{m}_o}{\pi \rho_f U_{eff}}} \tag{3}$$

being $\dot{m}_o$ and $\dot{M}_o$ the stationary mass flow and momentum flux at the nozzle outlet, ρ_f the fuel density, U_{eff} the effective outlet velocity and D_{eff} the effective outlet diameter

2.3   **Optical diagnostics**

A single-cylinder two stroke engine is used for visualization studies (Figure 1). In the particular configuration used for the study, an extended combustion chamber is located in place of the cylinder head. This combustion chamber is designed to hold the injector in one of the walls, plus up to three optical accesses in the rest of the sides. The top section of the engine is used to evacuate the exhaust gases. Additionally, an intermediate piece is designed to uniformly distribute the gases from the compression into this extended combustion chamber, so that a nearly quiescent environment is generated. More details of the optical engine can be seen in [36].

Table 2.B shows the test matrix conditions used for all the spray combustion visualization studies in terms of injection parameters and thermodynamic conditions at the engine Top Dead Center (TDC). Long injections have been used in all cases to ensure that steady-state conditions are reached during the injection event. In all cases, the engine runs at 500 rpm and the injection event is produced slightly before TDC, so

that the range of variation of the cylinder pressure during the measurements is minimized.

2.3.1. Mie-scattering

Liquid spray visualization has been characterized by means of Mie-scattering technique. In this case, a high-power continuous light source has been directed into the combustion chamber of the optical engine, and PCO- PixelFly digital camera has recorded the light scattered by the fuel droplets inside the spray. For these measurements, a non-reacting environment has been setup in the engine by using nitrogen instead of air as a working fluid. An example of the images obtained is available in Figure 2.a. More details about the experimental arrangement can be seen in [37].

2.3.2. Schlieren

A double-pass Schlieren technique has been used to characterize the vapor spray characteristics. In this case, the light emitted is passed first through a lens, creating a point focal light source. Then the light passes through a beam splitter and a collimating lens, creating a parallel light stream that enters the engine through the optical access. A metal mirror, attached to the injector holder, reflects the light beams arriving to it, which are then directed by the beam splitter to the CCD camera sensor, placed at 90º. Before arriving to the sensor, the light passes again through a lens, creating a focal point, where the light is spatially filtered by a knife edge that blocks a portion of the light beams. Under this configuration, the intensity acquired by the camera is related to the density inside the chamber. A sample image is provided in Figure 2.b. More details of this technique can be found in [30].

2.3.3. OH- chemiluminescence

OH- chemiluminescence technique is based on the light emission characteristics of the OH- radicals formed inside the diesel flames. In particular, it is known that the light emitted by this species is maximum in a characteristic wavelength (λ) of approximately 310 nm, dominating the total light emitted in this frequency. Thus, by visualizing the diffusion flame with an optical filter designed for a narrow band around this wavelength, it is possible to distinguish OH- radicals from other components of the flame. Nevertheless, the total amount of light emitted is relatively small, so an intensified ICCD camera has to be used. More details of the experimental technique are available in [32].

In the case of the current experiments, a LaVision-Dinamight with a resolution of 512 x 512 pixels was employed. An intensification level of 95% and an exposure time of 20 µs were selected with the aim of maximizing the signal-to-noise ratio while avoiding saturation of the camera sensor. The time step is set at 30 µs for an injection pressure of 30 MPa, and 20 µs for higher pressure levels, due to the higher injection velocity. Three repetitions are acquired for every time step. The kind of images obtained can be seen in Figure 2.c.

3. 1D SPRAY MODEL

The one-dimensional spray model used along the current study is based on two main assumptions:

- The analogy between a diesel spray and a turbulent gas jet, with the difference that the spray angle is not constant but depends on the particular nozzle geometry and injection conditions [38]–[41].

- Self-similarity of the radial profiles of the axial velocity and the fuel concentration inside the spray, which means that the velocity in any point of the spray can be defined using the following expressions:

$$U(x,r) = U(x,0)f(r/R_u) \qquad (4)$$

$$C(x,r) = C(x,0)[f(r/R_u)]^{Sc} \qquad (5)$$

Where *(x,r)* are the axial and radial positions inside the spray, $U(x,r)$ is the local axial velocity, $C(x,r)$ is the local fuel concentration, R_u is the spray radius at the axial distance x and Sc is the Schmidt number, which relates the viscous diffusion and mass diffusion rates.

Both hypotheses have been widely used and evaluated for high-pressure diesel sprays, showing good accuracy especially in the fully-developed region of the spray [42]–[46]. Starting from these hypotheses, and considering that steady state conditions are reached inside the nozzle, the momentum conservation equation between the nozzle outlet and a given section of the spray leads to:

$$\dot{M}_o = \dot{M}(x) = \int_0^{R_u} 2\pi\rho(x,r)rU^2(x,r)dr \qquad (6)$$

Where $\dot{M}_o$ is the momentum flux at the nozzle outlet; $\dot{M}(x)$ is the momentum flux at a section of the spray located at an axial distance x; and $\rho(x,r)$ is the local spray density.

The local spray density can be correlated to the local fuel concentration/mass fraction $C(x,r)$ by the use of the following expression:

$$\rho(x,r) = \rho_f \frac{1}{C(x,r)\left(1 - \frac{\rho_f}{\rho_a}\right) + \frac{\rho_f}{\rho_a}} \qquad (7)$$

Being ρ_f the liquid fuel density and ρ_a the ambient air density.

In order to develop equation 6, it is necessary to assume a certain radial distribution for the local spray velocity and concentration. For this purpose, numerous studies in the literature have made use of the analogy between liquid sprays and gas jets, which can be considered as a reasonable estimation out of the dense spray region [38], [43]. Based on this analogy, Gaussian profiles have been typically proposed [44], [47], [48]. For the current paper, the following expressions have been considered:

$$U(x,r) = U_{axis}(x) \cdot exp\left[-\alpha \left(\frac{r}{R_u}\right)^2\right] \tag{8}$$

$$C(x,r) = C_{axis}(x) \cdot exp\left[-\alpha \cdot Sc \left(\frac{r}{R_u}\right)^2\right] \tag{9}$$

Where $U_{axis}(x)$ and $C_{axis}(x)$ are the velocity and fuel concentration at the spray axis and α is a shape parameter for the Gaussian profile. Based on previous studies by the authors, values of $\alpha=4.605$ ([46]) and $Sc=0.5$ ([19], [48]) have been used for the current study.

Including equations (7-9) into (6) and resolving the differential equation, the following expression can be deduced:

$$\dot{M}_o = \frac{\pi}{2\alpha}\rho_a \cdot \tan^2\left(\frac{\theta_u}{2}\right)x^2 U_{axis}^2 \sum_{i=0}^{\infty}\frac{1}{\left(1+i\frac{Sc}{2}\right)}\left[C_{axis}\left(\frac{\rho_f - \rho_a}{\rho_f}\right)\right]^i \tag{10}$$

Where θ_u is the spray velocity angle, which can be related to the spray mass angle θ_m using the Schmidt number:

$$\tan(\theta_u) = \sqrt{Sc}\,\tan(\theta_m) \tag{11}$$

Finally, knowing that $C_{axis} = \left(\frac{U_{axis}}{U_{eff}}\right)^{1/Sc}$ (from the Schmidt number definition), equation (10) can be written as:

$$\dot{M}_o = \frac{\pi}{2\alpha} \rho_a \cdot Sc \cdot \tan^2\left(\frac{\theta_m}{2}\right) x^2 U_o^2 C_{axis}^{2Sc} \sum_{i=0}^{\infty} \frac{1}{\left(1 + i\frac{Sc}{2}\right)} \left[C_{axis}\left(\frac{\rho_f - \rho_a}{\rho_f}\right) \right]^i \quad (12)$$

From this equation, it is possible to determine the fuel concentration in the spray

axis at any given axial position once the spray momentum, the spray outlet velocity and

the spray mass angle are known. For the purpose of the current paper, the spray

momentum and the effective outlet velocity are determined from the hydraulic

characterization of the injector (as described in Section 2), while the spray mass angle is

assumed to be equal to the vapor spray angle obtained from the Schlieren images.

In order to numerically solve equation (12), it is necessary first to define a certain

number of terms for the series on the right hand side of the equation. Figure 3 shows a

sensitivity study on the influence of this parameter. As it can be seen, applying low

number of terms in the series results in an overestimation of the so called intact core

length of the spray, which is defined as the maximum axial position on which the fuel

concentration in the axis is equal to 1. When the number of terms increase, the solutions

tend to approach each other. Based on these results, a value of 7 terms has been chosen

for the rest of the study as the best tradeoff between model accuracy and velocity of

calculation.

4. EXPERIMENTAL RESULTS

4.1. Hydraulic characterization

Figure 4 shows the hydraulic behavior of the three nozzles of study in terms of the mass

flow (left) and momentum flux (right) at the outlet of each nozzle orifice at maximum

needle lift conditions. At low injection pressure, nozzle N3 shows the highest values of

mass flow due to its higher geometrical diameter. As injection pressure increases,

cavitation takes place in N3 due to its cylindrical shape, and consequently mass flow

collapse induced by cavitation appears. This makes that, for high injection pressures, the three nozzles deliver similar flow. In terms of momentum flux, the results seem to be aligned with the degree of convergence of the nozzles. This is consistent with the fact that for more convergent nozzles the flow suffers less detachment at the orifice inlet, which results in lower inlet pressure losses and higher outlet velocity.

These conclusions can be more clearly seen when looking at the effective outlet velocity and diameter (Figure 5). As previously stated, the effective outlet velocity is mostly scaled with the degree of convergence of the nozzle, and justifies the differences seen in terms of momentum flux. Regarding the effective outlet diameter, at low injection pressure (30 MPa) the difference between the experimental values obtained and the geometrical diameters (represented in dashed lines in the figure) is in the range of 5-10 µm. This may be due to the combination of the effect of the recirculation zone at the nozzle orifice inlet and the relatively low turbulence level achieved at such low injection pressures, which both result in a non-square outlet velocity profile. As injection pressure gets higher, the effective diameter for the convergent nozzles is mostly constant, while the cylindrical nozzle (N3) shows a significant decrease induced by the appearance of cavitation.

4.2. Vapor spray angle

Schlieren visualization results can be used to determine the spray angle, which will be used as a way to estimate the spray mass angle used for the one-dimensional model (θ_m).

Figure 6 shows the results achieved for all the nozzles as a function of the pressure drop along the injector. In all cases, the vapor spray angle ranges 13-18 degrees, which are typical values for diesel sprays at the density levels tested in the current work [38], [49]. Regarding the comparison between the different nozzles, different conclusions can be

drawn depending on the injection pressure level. At 30 MPa, the conical nozzles show larger spray angles than the cylindrical, with N2 having the highest values for most conditions. This can be explained based on a previous work by Payri et al [50], where the spray angle was correlated to the hydraulic performance of the nozzles according to the following expression:

$$tan\left(\frac{\theta_m}{2}\right) = 0.8113 \cdot \left(\frac{\rho_a}{\rho_f}\right)^{0.3316} \cdot C_a^{7.319} \cdot \left(\frac{L}{D_o}\right)^{-0.1872} \tag{13}$$

Where C_a is the area coefficient, defined as the ratio between the effective outlet area and the geometrical area, L is the nozzle orifice length and D_o is the geometrical outlet diameter. According to the experimental results observed in Figure 5, average area coefficients for the 30 MPa case would be approximately 0.92, 0.91 and 0.88 for nozzles N1, N2 and N3, respectively. It can be clearly seen that N3 has the lowest area coefficient, which is consistent with the lower vapor angle results obtained. Regarding the conical nozzles, the area coefficient values are similar, and the differences among the nozzles can be explained thanks to the influence of L/D_o. Increasing the injection pressure, N3 starts being affected by cavitation formation inside the nozzle orifice, which is known to enhance atomization and fuel-air mixing processes from previous studies in the literature ([10], [51]). Consequently, the spray angle increases and N3 achieves the largest angle values for all the 80 and 160 MPa cases.

4.3. Liquid length

Figure 7 summarizes the results achieved in terms of stabilized liquid length. As it was expected, the liquid length shortens significantly when increasing the ambient temperature, as evaporation gets enhanced. Regarding the comparison between the nozzles, even if the results are not fully conclusive, it can be observed that the liquid length tends to be larger for nozzle N3, especially for mid-to-low injection pressures,

where it has the highest effective diameter. This is consistent with previous findings in the literature, which showed that the liquid length can be expressed as [52], [53]:

$$LL = \frac{k_s \cdot \left(\frac{1}{4}\right)^{1/2} \cdot \left(\frac{\pi}{4}\right)^{1/2} \cdot D_{eff}}{C_{mv} \cdot tan\left(\frac{\theta_u}{2}\right)} \left(\frac{\rho_f}{\rho_a}\right)^{1/2} \tag{14}$$

Where C_{mv} is the fuel concentration at the spray axis needed for reaching the complete evaporation of the fuel (i.e., the fuel concentration in the spray axis at the liquid length axial position). It has to be noted that the value of C_{mv} depends on combustion chamber temperature and the physical properties of the fuel, mostly the distillation characteristics. Furthermore, different fuels could lead to variations in the effective diameter (linked to the development of the flow turbulence) and on the spray angle, also affecting the liquid length.

As it can be seen in equation (14), liquid length tends to increase when increasing the effective diameter, as previously discussed. Nevertheless, the results in Figure 7 do not show a clear trend for nozzles N1 and N2, which are also affected by the effect of the nozzle geometry on the fuel-air mixing efficiency, characterized by the spray angle θ_u. If the liquid length is normalized by the effects of the effective diameter and the spray angle according to equation (14), it can be observed how all the values collapse and no clear trend with the nozzle geometry can be identified. Additionally, the normalized values are slightly higher for the low temperature results, due to the effect of the temperature on C_{mv}.

4.4. Ignition delay

Ignition delay has been obtained from the OH- chemiluminescence measurements, which are an indicator for the beginning of the high-temperature reactions into the combustion process. In particular, ignition delay has been defined as the time between

the Start of Injection (SOI) and the time at which 5% percentile of the cumulative OH-chemiluminescence intensity was reached.

Figure 9 shows the results of ignition delay as a function of the pressure drop. The most clear trends that can be identified are the reduction of the ignition delay as the pressure and density in the chamber increase. This is consistent with previous experiences in the literature, which report that ignition delay can be expressed in the form of an Arrhenius correlation [26], [29]:

$$\tau = A \cdot P_{back}^{-n} \cdot \exp\left(\frac{E_A}{R \cdot T}\right) \tag{15}$$

Where τ is the ignition delay, E_A is the activation energy and T is the temperature in the combustion chamber. In this expression, the influence of the pressure and temperature consider mostly the enhancement of the reaction rates into the chemical kinetics mechanism.

Additionally, in the experimental data it can also be observed that there is a trend to reduce the ignition delay when increasing the injection pressure, which tends to improve spray atomization and reduce the physical time needed for mixing and vaporizing. Similar results have also been observed for other diesel sprays studies in the literature [31], [54].

Regarding the influence of the nozzle geometry, it can be clearly seen that in the low temperature case, where chemical processes are slower in general, there are some differences among the nozzles, with N1 showing in general the largest ignition delays and similar values for the other two. In the high temperature case, similar trends are observed, but with smaller differences in absolute value. These trends are a consequence of the differences into the physical time needed for the fuel to atomize, mix with the air and evaporate. This time will be analyzed in more details in the next section.

5. LIQUID LENGTH CORRELATION AND PHYSICAL DELAY DETERMINATION

Equation (14) expressed the stabilized liquid length of a spray as a function of a characteristic concentration for mixing and vaporizing (C_{mv}). Starting from this definition, it is possible to define a characteristic time for mixing and vaporizing (t_{mv}), which would represent the time needed for a fuel parcel to travel from the nozzle outlet orifice up to the liquid length position:

$$t_{mv} = \frac{k_s \cdot \left(\frac{1}{4}\right)^{1/2} \cdot \left(\frac{\pi}{4}\right)^{1/2} \cdot D_{eff}}{C_{mv}^2 \cdot U_{eff} \cdot tan\left(\frac{\theta_u}{2}\right)} \left(\frac{\rho_f}{\rho_a}\right)^{1/2} \tag{16}$$

More details about the mathematical development and assumptions to reach to this expression can be found in [52].

In order to calculate the values of t_{mv}, it is necessary first to know the values of k_s and C_{mv}. For this purpose, the 1D spray model presented in section 3 will be used. In particular, C_{mv} can be estimated from the numerical solution of equation (12) particularized for $x=LL$. To approach this solution, the spray momentum $\dot{M}_o$ will be the experimental value obtained from the momentum flux measurements and θ_m will be estimated from the vapor spray angle results. The results from these calculations can be seen in Figure 10. As it was expected, the results of C_{mv} are very similar for all the nozzles, with a small dispersion linked to the experimental uncertainties, while there is a clear trend with respect to the chamber temperature, due to the enhanced evaporation efficiency. In particular, the value of C_{mv} goes from a value of approximately 0.2 for the temperature of 790 K to approximately 0.23 for the 935 K case, which represents an

increase of around 1% in the characteristic fuel concentration for every 10 K

temperature grow.

Figure 11 shows the comparison of two different correlations from the liquid length.

First, the liquid length experimental results have been adjusted to the following

expression based on previous literature studies [52]:

$$LL = cns \cdot D_{eff} \cdot \rho_a^{-0.5} \cdot T^a \cdot \Delta P^b \qquad (17)$$

Where ΔP is the pressure drop defined as $P_{inj} - P_{back}$. For the particular case of the

current studies, coefficients of -1.64 and -0.52 have been obtained for the values of a

and b, resulting in an overall R-squared value of 79.5%.

Then, a correlation directly based on equation (14) has been obtained. The results a

summarized in Figure 11. In this correlation, it has been chosen to let as the only fitting

parameter the value of k_s. Doing so, an average value of 1.254 has been obtained. This

value for the spray constant is very similar to the value of 1.26 obtained on previous

studies based on spray penetration analysis [43]. The R-squared for this second

correlation is significantly increased compared to the previous correlation, up to a value

of 90.9%, which is an indication of the consistency of the values of k_s and C_{mv} achieved

using this methodology. Despite this improvement, it has to be considered that the value

achieved is still relatively low, probably due in part to uncertainties into the fuel

temperature during the injection, which are known to have an impact on the evaporation

characteristics [53].

Once the values of the spray constant k_s and the mixing and vaporization concentration

C_{mv} have been estimated, it is possible to use it to calculate the characteristic time for

mixing and vaporizing, according to equation (16). The results from this procedure are

depicted in Figure 12. Two main conclusions can be drawn from this graph. First, it can

be seen how the trends observed in terms of t_{mv} are similar to those achieved for the

overall ignition delay (i.e., a nozzle characterized by higher t_{mv} is also showing longer ignition delay, and viceversa). In particular, it can be seen how N3, despite having largest effective diameter and lower effective velocity than the convergent nozzles (which would result in longer physical time values according to equation 16), is capable to achieve similar or even lower t_{mv} values thanks to the beneficial effect of cavitation into the spray angle. Nevertheless, it shall be noted that the differences observed in t_{mv} are generally lower compared to those observed in the ignition delay. This suggests that the influence of the physical processes on the ignition delay is not only linked to the physical delay induced by the mixing and vaporizing processes, but also to the distribution of local equivalence ratio inside the spray, which can also affect autoignition processes.

The second conclusion is related to the fact that even in the case of a diesel spray, which is characterized by a relatively high reactivity, the time needed for the physical processes is relatively small compared to the total ignition delay. This is particularly true when combining low values of chamber pressure and temperature, which slows chemical kinetics down, with high injection pressures, which tends to enhance the physical processes thanks to the higher spray momentum. Under such conditions, the time to mix and vaporize represents only around a 5% on the total ignition delay. In the opposite case (high thermodynamic conditions and low injection pressure), the physical delay can represent up to 30% of τ.

6. IGNITION DELAY CORRELATION

Figure 13 and Table 3 show the result of two different ignition delay correlations for the data obtained along this study. In the left hand side of the figure, a typical Arrhenius correlation like the one introduced in equation (18) has been obtained:

$$\tau = A \cdot P_{back}^{-n} \cdot \exp\left(\frac{E_A}{R \cdot T}\right) \cdot P_{inj}^{-m} \tag{18}$$

On the right hand side, the Arrhenius correlation has been modified to include the effect of the physical delay estimated by the value of t_{mv}. The first aspect to be highlighted is that both correlations show similar values of standard R-squared and adjusted R-squared parameters. This can be seen as an indication that the number of experiments performed, even if reduced (12 conditions per nozzle, 36 in total), is still reasonable for the kind of correlation proposed. While both correlations show a good agreement with the experimental data, which can be seen in terms of the high R-squared values achieved, it is visible how the new correlation is more capable to reproduce the experimental data, resulting in a narrower observed vs. predicted trend. It is also noticeable how after introducing the value of t_{mv}, the exponent of the injection pressure on the ignition delay correlation reduces, since the most important effects of this parameter are already captured into the t_{mv} term. Nevertheless, there is still a statistically relevant influence of the injection pressure on the ignition delay data, which is again an indication that there is an influence of the fuel injection processes that is not fully captured by the physical delay calculation previously described.

Figure 14 shows the comparison of the two correlations in terms of an accuracy coefficient in terms of the ignition delay, defined as:

$$\tau_{accuracy} = \frac{\left|\tau_{exp} - \tau_{ini}\right| - \left|\tau_{exp} - \tau_{new}\right|}{\tau_{exp}} \cdot 100 \tag{19}$$

Being τ_{ini} and τ_{new} the ignition delay values estimated with the initial (w/o t_{mv}) and new (w/ t_{mv}) correlations, respectively. With this definition, a positive value of the accuracy coefficient implies that the deviation of the initial correlation with respect to the experiments is higher than the new one, which represents an improvement for the new formulation.

Looking at the results from Figure 14, it can be stated that the new correlation improves the accuracy of the ignition delay prediction for most of the experimental conditions. The maximum improvement achieved is of approximately 4%, while the maximum deterioration does not exceed 2% and appears in few operating conditions. Thus, it can be concluded that the correlation including the time for mixing and vaporizing is confirmed as a better representation of the ignition delay experimental results, since it can take into account the differences induced by the different nozzle geometries. Nevertheless, it has to be noted that the impact of the new proposed methodology is limited in this case due to the fact that the three nozzles used for the study have similar hydraulic characteristics, as seen in figures 4 and 5. Future work will consider the extension of this methodology to nozzles with higher geometrical and hydraulic differences, for which the impact of the physical delay could be more significant. Additionally, the usage of fuels with different physical and chemical properties will also be considered.

7. CONCLUSIONS

In the current paper, a study about the influence of the nozzle geometry on the injector hydraulics, evaporative spray formation and ignition characteristics of diesel sprays has been performed. For this purpose, three multi-hole nozzles characterized by different degrees of conicity (k-factor of 2, 1.6 and 0) have been analyzed.

First of all, measurements of injection rate and momentum flux have been performed, allowing to characterize the nozzles in terms of the effective outlet velocity and diameter. From these measurements, it was observed that the effective velocity is tightly linked to the nozzle conicity, due to the lower inlet pressure drop, while the effective

diameter is mostly affected by cavitation formation inside the nozzle for the cylindrical nozzles.

Schlieren and Mie-scattering visualization tests were performed to characterize the vapor spray angle and the stabilized liquid length for diesel sprays injected into an optically accessible 2-stroke diesel engine. The vapor spray angle was observed to be similar for the conical nozzles, while the cylindrical showed slightly higher values for mid-to-high injection pressure levels, thanks to the effect of cavitation. Regarding liquid length, the results were observed to be mostly dependent on the nozzle effective diameter and the vapor spray angle.

The combination of the previous results with a 1-dimensional spray model based on the gas-jet analogy has allowed to determine a characteristic fuel concentration at the liquid length position. It has been observed that this concentration depends on the chamber temperature, while the effect of the nozzle geometry and other boundary conditions is limited. The definition of this characteristic concentration was used to determine a new correlation for the stabilized liquid length, which proved to be capable to improve the accuracy of the predictions given by other correlations in the literature. Additionally, it was possible to estimate the time needed for a fuel parcel to reach this characteristic concentration in the spray axis (defined as t_{mv}), and this time was used as an indicator of the physical delay associated with mixing and evaporation phenomena into the diesel spray combustion processes. It could be seen that this time was generally shorter for the cylindrical nozzle thanks to the benefits of cavitation on atomization and fuel-air mixing processes, even despite the higher effective diameter and lower outlet velocity characteristic of this nozzle compared to the cylindrical ones.

Finally, ignition delay was obtained from OH- chemiluminescence measurements. The results showed that there is a non-negligible influence of the nozzle geometry in the

ignition delay, especially at low ambient temperature conditions, which is consistent to the physical delay results previously attained. Two experimental Arrhenius correlations for the ignition delay have been evaluated: one including only the influence of the chamber thermodynamic conditions and the injection pressure, as typically seen in the literature, and another which includes also the physical delay previously calculated. The results show that the new correlation improves the ignition delay accuracy for most conditions, as it is more capable to capture the differences among the nozzles.

ACKNOWLEDGMENTS

REFERENCES

[1] T. V. Johnson, "Vehicular Emissions in Review," *SAE Int. J. Engines*, vol. 5, no. 2, pp. 2012-01–0368, 2012.

[2] P. C. Miles, L. Hildingsson, and A. Hultqvist, "The influence of fuel injection and heat release on bulk flow structures in a direct-injection, swirl-supported diesel engine," *Exp. Fluids*, vol. 43, no. 2–3, pp. 273–283, 2007.

[3] Z. Zheng, X. Tian, and X. Zhang, "Effects of split injection proportion and the second injection time on the mixture formation in a GDI engine under catalyst heating mode using stratified charge strategy," *Appl. Therm. Eng.*, vol. 84, pp. 237–245, Jun. 2015.

[4] A. Maghbouli, T. Lucchini, G. D'Errico, and A. Onorati, "Effects of grid

alignment on modeling the spray and mixing process in direct injection diesel engines under non-reacting operating conditions," *Appl. Therm. Eng.*, vol. 91, pp. 901–912, 2015.

[5]   D. Kim, J. Martz, and A. Violi, "Effects of fuel physical properties on direct injection spray and ignition behavior," *Fuel*, vol. 180, pp. 481–496, 2016.

[6]   Y. Pei, E. R. Hawkes, M. Bolla, S. Kook, G. M. Goldin, Y. Yang, S. B. Pope, and S. Som, "An analysis of the structure of an n-dodecane spray flame using TPDF modelling," *Combust. Flame*, vol. 168, pp. 420–435, 2016.

[7]   W. Ning, R. D. Reitz, R. Diwakar, and A. M. Lippert, "A Numerical Investigation of Nozzle Geometry and Injection Condition Effects on Diesel Fuel Injector Flow Physics," *SAE Tech. Pap. 2008-01-0936*, 2008.

[8]   C. Yao, P. Geng, Z. Yin, J. Hu, D. Chen, and Y. Ju, "Impacts of nozzle geometry on spray combustion of high pressure common rail injectors in a constant volume combustion chamber," *Fuel*, vol. 179, pp. 235–245, Sep. 2016.

[9]   F. Brusiani, S. Falfari, and P. Pelloni, "Influence of the diesel injector hole geometry on the flow conditions emerging from the nozzle," *Energy Procedia*, vol. 45, pp. 749–758, 2014.

[10]   J. M. Desantes, R. Payri, F. J. Salvador, and J. De la Morena, "Influence of cavitation phenomenon on primary break-up and spray behavior at stationary conditions," *Fuel*, vol. 89, no. 10, pp. 3033–3041, 2010.

[11]   O. Oguz and M. Ergeneman, "Effect of nozzle dimensions and fuel type on flame lift-off length," *Fuel*, vol. 115, pp. 833–840, 2014.

[12]   S. Som, A. I. Ramírez, D. E. Longman, and S. K. Aggarwal, "Effect of nozzle orifice geometry on spray, combustion, and emission characteristics under diesel engine conditions," *Fuel*, vol. 90, no. 3, pp. 1267–1276, 2011.

[13] T. Hulkkonen, T. Sarjovaara, O. Kaario, I. Hamalainen, and M. Larmi, "Experimental Study of Conical Diesel Nozzle Orifice Geometry," *At. Sprays*, vol. 25, no. 6, pp. 519–538, 2015.

[14] R. Payri, F. J. Salvador, M. Carreres, and J. De la Morena, "Fuel temperature influence on the performance of a last generation common-rail diesel ballistic injector. Part II: 1D model development, validation and analysis," *Energy Convers. Manag.*, vol. 114, pp. 376–391, Apr. 2016.

[15] E. Plamondon and P. Seers, "Development of a simplified dynamic model for a piezoelectric injector using multiple injection strategies with biodiesel/diesel-fuel blends," *Appl. Energy*, vol. 131, pp. 411–424, 2014.

[16] R. Marcer, C. Audiffren, A. Viel, B. Bouvier, A. Walbott, and B. Argueyrolles, "Coupling 1D System AMESim and 3D CFD EOLE models for Diesel Injection Simulation Renault," in *ILASS - Europe 2010, 23rd Annual Conference on Liquid Atomization and Spray Systems*, 2010, no. September, pp. 1–10.

[17] J. V. Pastor, J. J. Lopez, J. M. Garcia-Oliver, and J. M. Pastor, "A 1D model for the description of mixing-controlled inert diesel sprays," *Fuel*, vol. 87, no. 13–14, pp. 2871–2885, 2008.

[18] M. Costa, U. Sorge, and L. Allocca, "Increasing energy efficiency of a gasoline direct injection engine through optimal synchronization of single or double injection strategies," *Energy Convers. Manag.*, vol. 60, pp. 77–86, 2012.

[19] F. J. Salvador, S. Ruiz, J. Gimeno, and J. De la Morena, "Estimation of a suitable Schmidt number range in diesel sprays at high injection pressure," *Int. J. Therm. Sci.*, vol. 50, no. 9, pp. 1790–1798, 2011.

[20] J. De la Morena, K. Neroorkar, A. H. Plazas, R. C. Peterson, and D. P. Schmidt, "Numerical analysis of the influence of diesel nozzle design on internal flow

characteristics for 2-valve diesel engine application," *At. Sprays*, vol. 23, no. 2, pp. 97–118, 2013.

[21] F. J. Salvador, M. Carreres, D. Jaramillo, and J. Martínez-López, "Comparison of microsac and VCO diesel injector nozzles in terms of internal nozzle flow characteristics," *Energy Convers. Manag.*, vol. 103, pp. 284–299, 2015.

[22] K. Saha, S. Som, M. Battistoni, Y. Li, S. Quan, and P. K. Senecal, "Numerical simulation of internal and near-nozzle flow of a gasoline direct injection fuel injector," *J. Phys. Conf. Ser.*, vol. 656, no. January 2016, p. 12100, 2015.

[23] B. Yin, S. Yu, H. Jia, and J. Yu, "Numerical research of diesel spray and atomization coupled cavitation by Large Eddy Simulation (LES) under high injection pressure," *Int. J. Heat Fluid Flow*, vol. 59, pp. 1–9, 2016.

[24] F. J. Salvador, J. V. Romero, M. D. Roselló, and D. Jaramillo, "Numerical simulation of primary atomization in diesel spray at low injection pressure," *J. Comput. Appl. Math.*, vol. 291, pp. 94–102, 2016.

[25] Y. Wang, L. Qiu, R. D. Reitz, and R. Diwakar, "Simulating cavitating liquid jets using a compressible and equilibrium two-phase flow solver," *Int. J. Multiph. Flow*, vol. 63, pp. 52–67, 2014.

[26] S. K. Aggarwal, "A review of spray ignition phenomena: Present status and future research," *Prog. Energy Combust. Sci.*, vol. 24, no. 95, pp. 565–600, 1998.

[27] Y. M. Wright, O. N. Margari, K. Boulouchos, G. De Paola, and E. Mastorakos, "Experiments and simulations of n-heptane spray auto-ignition in a closed combustion chamber at diesel engine conditions," *Flow, Turbul. Combust.*, vol. 84, no. 1, pp. 49–78, 2010.

[28] A. E. Dhole, R. B. Yarasu, and D. B. Lata, "Investigations on the combustion duration and ignition delay period of a dual fuel diesel engine with hydrogen and

producer gas as secondary fuels," *Appl. Therm. Eng.*, vol. 107, pp. 524–532, 2016.

[29] D. N. Assanis, Z. S. Filipi, S. B. Fiveland, and M. Syrimis, "A predictive ignition delay correlation under steady-state and transient operation of a direct injection diesel engine," *J. Eng. Gas Turbines Power*, vol. 125, no. 2, pp. 450–457, 2003.

[30] R. Payri, J. Gimeno, G. Bracho, and D. Vaquerizo, "Study of liquid and vapor phase behavior on Diesel sprays for heavy duty engine nozzles," *Appl. Therm. Eng.*, vol. 107, pp. 365–378, 2016.

[31] F. Pischinger, U. Reuter, and E. Scheid, "Self-Ignition of Diesel Sprays and Its Dependence on Fuel Properties and Injection Parameters," *Eng. Gas Turbines Power*, vol. 110, no. 3, pp. 399–404, 1988.

[32] R. Payri, F. J. Salvador, J. Gimeno, and J. De la Morena, "Effects of nozzle geometry on direct injection diesel engine combustion process," *Appl. Therm. Eng.*, vol. 29, no. 10, pp. 2051–2060, 2009.

[33] W. Bosch, "The Fuel Rate Indicator: a New Measuring Instrument for Display of the Characteristics of Individual Injection," *SAE Pap. 660749*, 1966.

[34] R. Payri, F. J. Salvador, J. Gimeno, and G. Bracho, "A new methodology for correcting the signal cumulative phenomenon on injection rate measurements," *Exp. Tech.*, vol. 32, no. February, pp. 46–49, 2008.

[35] R. Payri, J. M. Garcia-Oliver, F. J. Salvador, and J. Gimeno, "Using spray momentum flux measurements to understand the influence of diesel nozzle geometry on spray characteristics," *Fuel*, vol. 84, no. 5, pp. 551–561, 2005.

[36] V. Bermúdez, J. M. Garcia-Oliver, E. Juliá, and S. Martínez-Martínez, "Engine with optically accessible cylinder head: a research tool for injection and combustion processes," *SAE Tech. Pap. 2003-01-1110*, 2003.

[37]   R. Payri, F. J. Salvador, A. Garcia, and A. Gil, "Combination of visualization techniques for the analysis of evaporating diesel sprays," *Energy & Fuels*, vol. 26, pp. 5481–5490, 2012.

[38]   J. D. Naber and D. L. Siebers, "Effects of Gas Density and Vaporization on Penetration and Dispersion of Diesel Sprays," in *SAE Paper 960034*, 1996, vol. 105, no. 412, pp. 82--111.

[39]   G. E. Cossali, A. Geria, A. Coghe, and G. Brunello, "Effect of Gas Density and Temperature on Air Entrainment in a Transient Diesel Spray," *SAE Pap. 960862*, no. 412, 1996.

[40]   R. D. Reitz and F. V. Bracco, "On the dependence of spray angle and other spray parameters on nozzle design and operating conditions," *SAE Pap. 790494*, 1979.

[41]   F. Payri, R. Payri, M. Bardi, and M. Carreres, "Engine combustion network: Influence of the gas properties on the spray penetration and spreading angle," *Exp. Therm. Fluid Sci.*, vol. 53, no. September 2015, pp. 236–243, 2014.

[42]   C. M. V Prasad and S. Kar, "An investigation on the diffusion of momentum and mass of fuel in a Diesel fuel spray," *ASME J Eng Power*, pp. 1–11, 1976.

[43]   J. M. Desantes, R. Payri, F. J. Salvador, and A. Gil, "Development and validation of a theoretical model for diesel spray penetration," *Fuel*, vol. 85, no. 7–8, pp. 910–917, 2006.

[44]   J. O. Hinze, *Turbulence*. McGraw-Hill New York, 1975.

[45]   A. H. Lefèbvre, *Atomization and Sprays*. CRC, 1989.

[46]   J. M. Desantes, R. Payri, J. M. Garcia-Oliver, and F. J. Salvador, "A contribution to the understanding of isothermal diesel spray dynamics," *Fuel*, vol. 86, no. 7–8, pp. 1093–1101, 2007.

[47]   H. Schlichting, *Boundary-Layer Theory*. McGraw-Hill, 1978.

[48]   J. M. Desantes, F. J. Salvador, J. J. Lopez, and J. De la Morena, "Study of mass and momentum transfer in diesel sprays based on X-ray mass distribution measurements and on a theoretical derivation," *Exp. Fluids*, vol. 50, no. 2, pp. 233–246, 2011.

[49]   S. Huang, P. Deng, R. Huang, Z. Wang, Y. Ma, and H. Dai, "Visualization research on spray atomization, evaporation and combustion processes of ethanol-diesel blend under LTC conditions," *Energy Convers. Manag.*, vol. 106, pp. 911–920, 2015.

[50]   R. Payri, F. J. Salvador, J. Gimeno, and R. Novella, "Flow regime effects on non-cavitating injection nozzles over spray behavior," *Int. J. Heat Fluid Flow*, vol. 32, no. 1, pp. 273–284, 2010.

[51]   A. Andriotis and M. Gavaises, "Influence of vortex flow and cavitation on near-nozzle diesel spray dispersion angle," *At. Sprays*, vol. 19, no. 3, pp. 247–261, 2009.

[52]   R. Payri, F. J. Salvador, J. Gimeno, and L. D. Zapata, "Diesel nozzle geometry influence on spray liquid-phase fuel penetration in evaporative conditions," *Fuel*, vol. 87, no. 7, pp. 1165–1176, 2008.

[53]   D. L. Siebers, "Scaling liquid-phase fuel penetration in diesel sprays based on mixing-limited vaporization," *SAE Tech. Pap. 1999-01-0528*, 1999.

[54]   R. Payri, F. J. Salvador, J. Manin, and A. Viera, "Diesel ignition delay and lift-off length through different methodologies using a multi-hole injector," *Appl. Energy*, vol. 162, pp. 541–550, 2016.

LIST OF TABLES

FIGURE CAPTIONS

Table 1. Physical and chemical properties of Repsol CEC RF-06-99 fuel.

Test	Unit	Result	Uncertainty	Methodology
Density at 15ºC	Kg/m^3	843	±0.2	EN ISO 12185/96
Viscosity at 40ºC	mm^2/s	2.847	±0.42	EN ISO 3104/99
Volatility				
65% distillated at	ºC	294.5	±3.7	EN ISO 3405:01
85% distillated at	ºC	329.2	±3.7	
95% distillated at	ºC	357.0	±3.7	
Cetane Number	------	51.52	± 2.5	
Cetane Index	------	49.6	± 0.51	
Calorific Value				
Higher Calorific Value	MJ/kg		45.58	ASTM D-240/02
Lower Calorific Value	MJ/kg		42.78	ASTM D-240/02
Fuel molecular composition		C$_{13}$H$_{28}$		

Table 2. Experimental test matrix.

Injection			Chamber conditions		
P$_{inj}$ [MPa]	E.T. [ms]	SOE [degBTDC]	P. at TDC [MPa]	T at TDC [K]	Density [Kg/m^3]
A. Hydraulic tests (injection rate and spray momentum)					
30	2	-	3	298	33.9*
30	2	-	5	298	56.5*
30	2	-	7	298	79*
30	2	-	9	298	101.7*
80	1	-	3	298	33.9*
80	1	-	5	298	56.5*
80	1	-	7	298	79*
80	1	-	9	298	101.7*
160	1	-	3	298	33.9*
160	1	-	5	298	56.5*
160	1	-	7	298	79*
160	1	-	9	298	101.7*
B. Spray visualization tests (Mie-scattering, Schlieren and OH-chemiluminescence)					
30	2	6	5	950	18
30	2	6	5	800	22
30	2	6	7	950	26
30	2	6	7	800	30
80	1	4	5	950	18
80	1	4	5	800	22
80	1	4	7	950	26
80	1	4	7	800	30
160	1	3	5	950	18
160	1	3	5	800	22
160	1	3	7	950	26
160	1	3	7	800	30

* Calculated for nitrogen atmosphere on spray momentum tests

Table 3: Ignition delay correlations summary

a. Initial correlation			b. New correlation (including t_{mv})	
EXP.	**FIT**	**Confidence Interval**	**FIT**	**Confidence Interval**
A	0.26	[0.18, 0.34]	0.17	[0.09, 0.26]
n	0.89	[0.74, 1.04]	0.98	[0.81, 1.15]
E_A/R	2510.9	[2227, 2795]	2688.1	[2357, 2957]
m	0.138	[0.11, 0.17]	0.079	[0.035, 0,11]
R-Squared= 94.8 %			R-Squared= 95.3 %	
Adjusted R-Squared= 94.4 %			Adjusted R-Squared= 94.9 %	

FIGURES
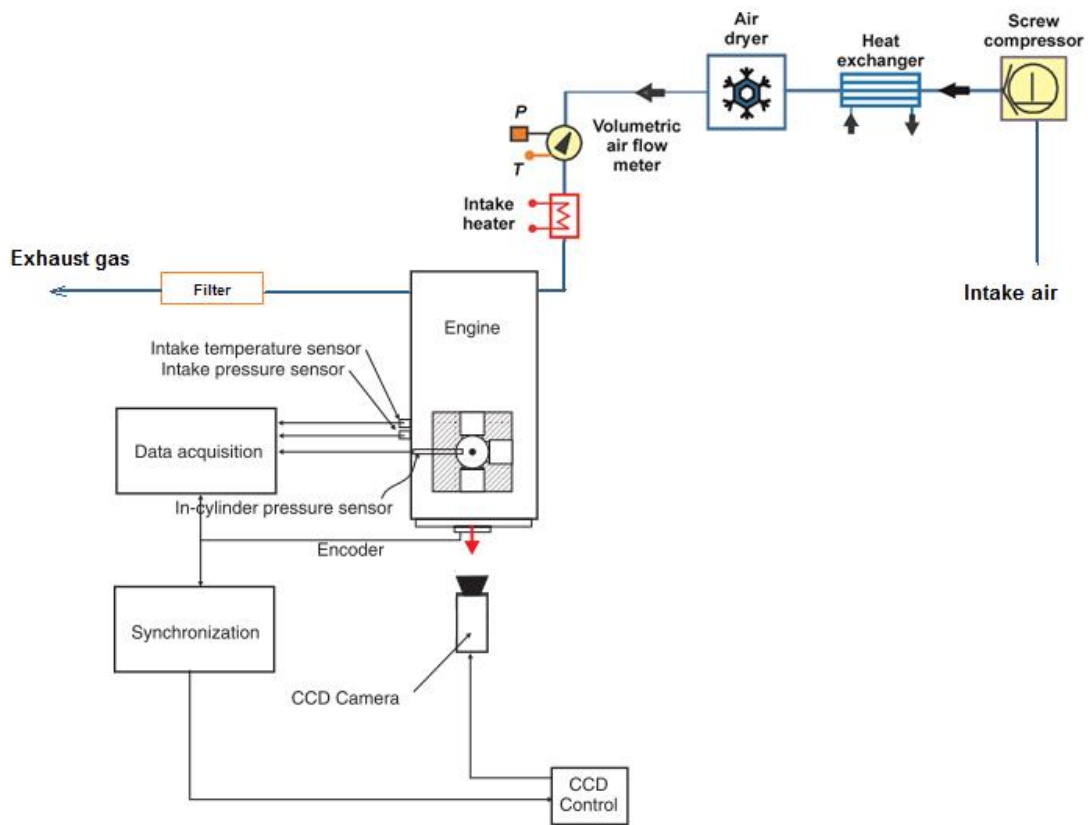
Figure 1: 2-stroke optical single-cylinder engine test bench

P_{inj} = 80 MPa

T=935 K, P_{back}=50 MPa$\Rightarrow$ 18 kg/m^3

b) Schlieren

a) Mie-scattering

c) OH- chemiluminescence
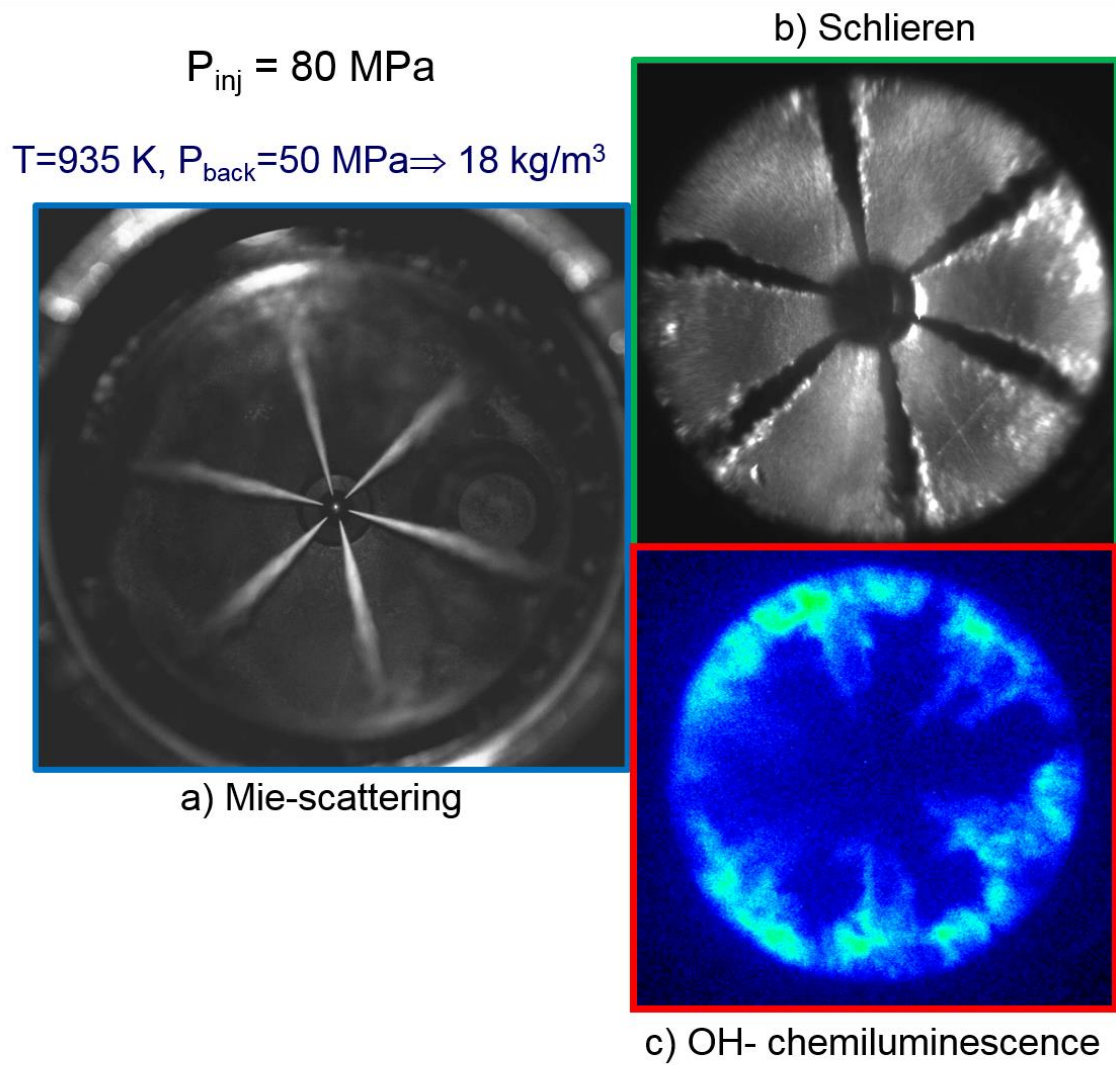
Figure 2: Sample images from experimental optical diagnostics. a) Mie-scattering,

b) Schlieren, c) OH- chemiluminescence
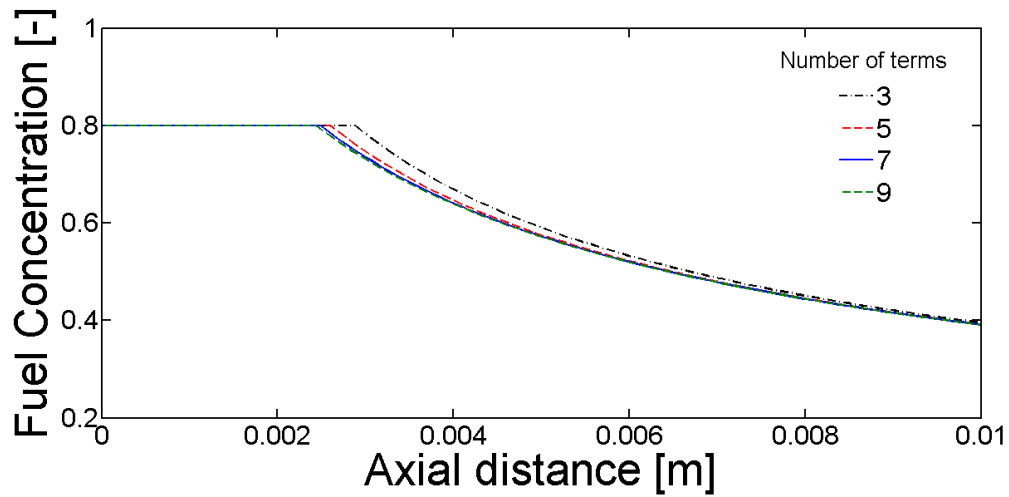
Figure 3: Influence of the number of terms in the spray model numerical series
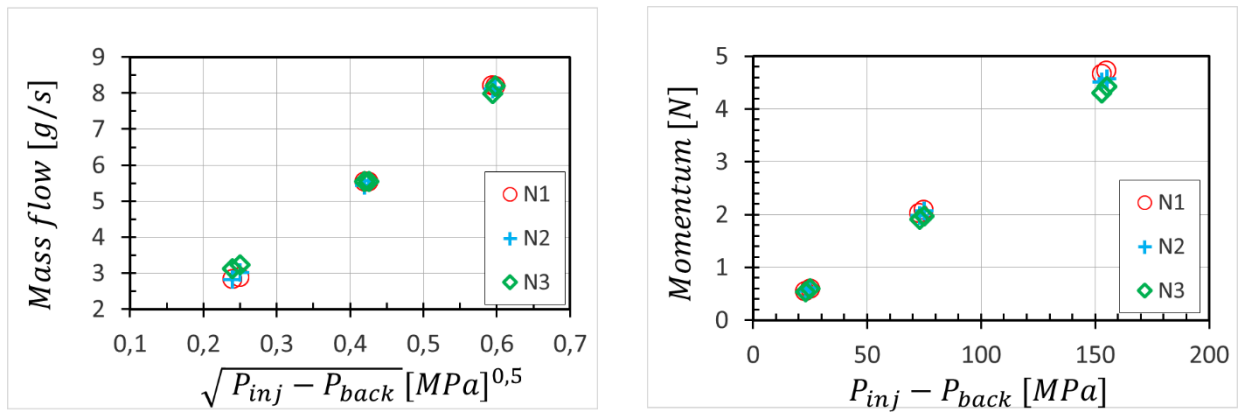
Figure 4: Stationary mass flow rate and momentum flux results
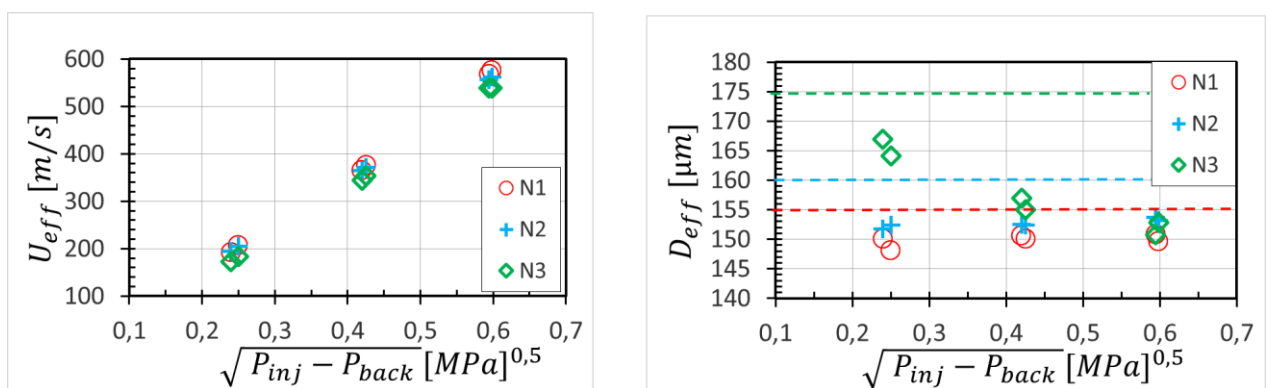
Figure 5: Effective outlet velocity and diameter results.
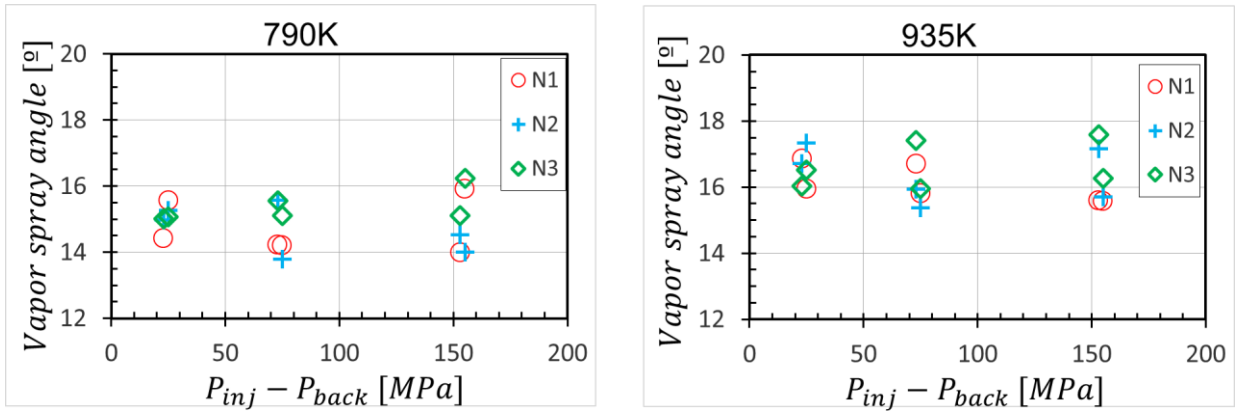
Figure 6: Vapor spray angle vs pressure drop
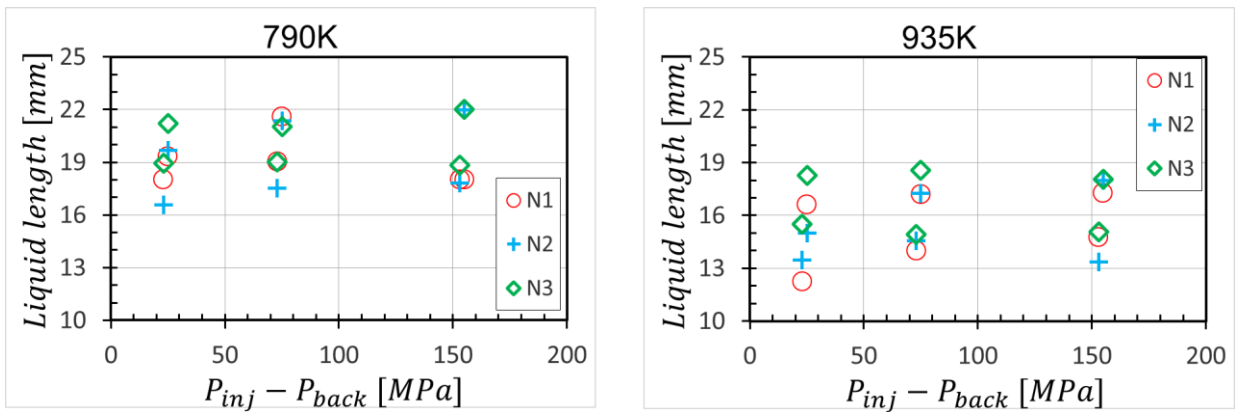
Figure 7: Stabilized liquid length vs pressure drop
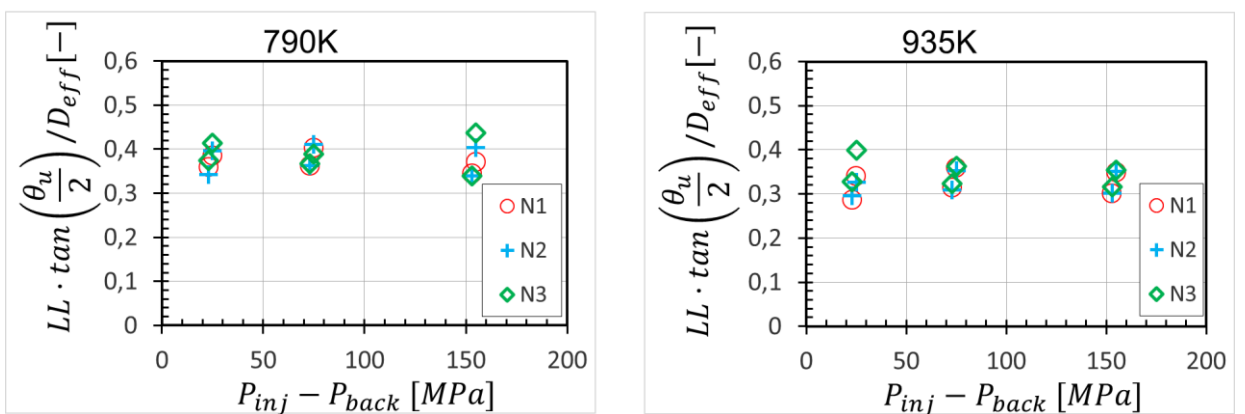
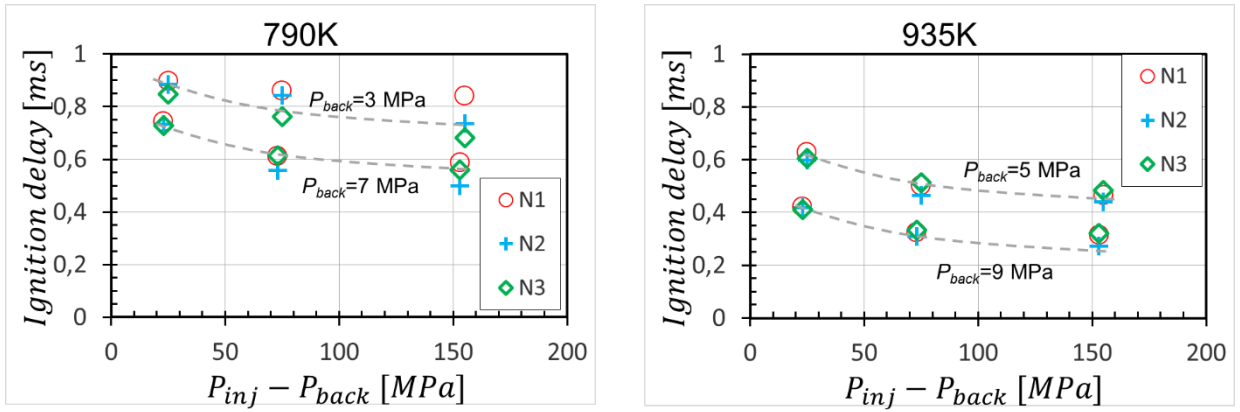Figure 8: Normalized stabilized liquid length vs pressure drop

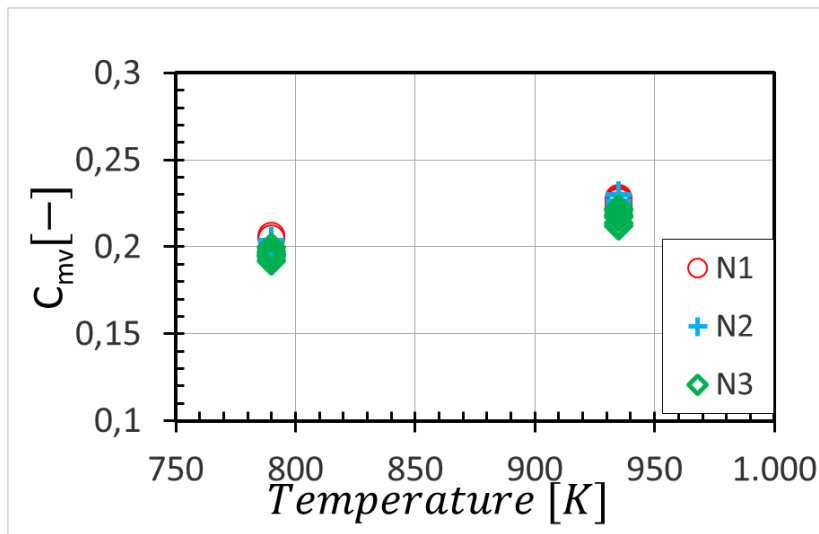Figure 9: Ignition delay vs pressure drop

Figure 10: Fuel concentration for mixing and vaporizing (C_{mv}) as a function of
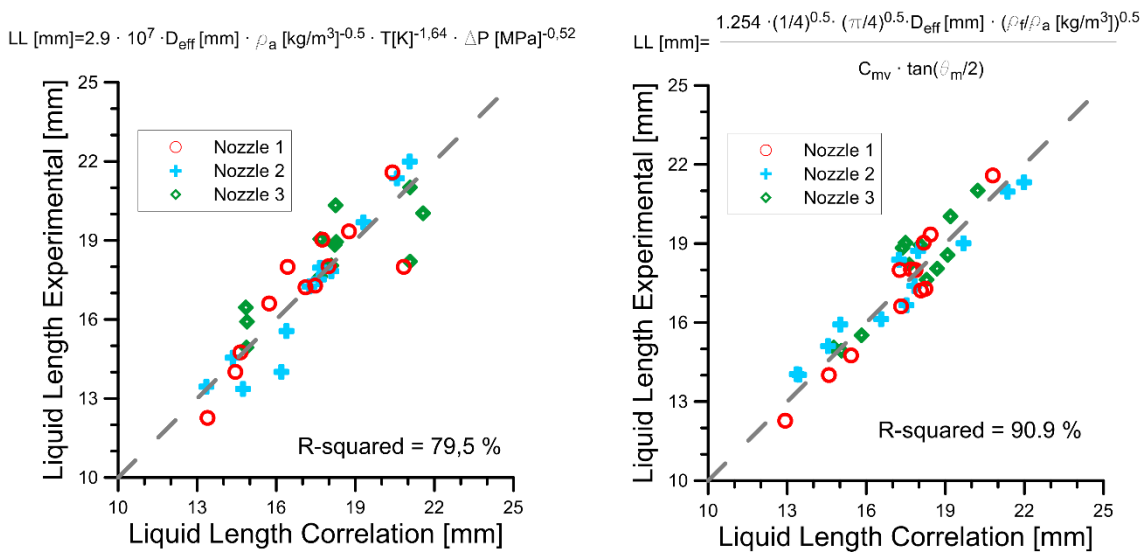
temperature

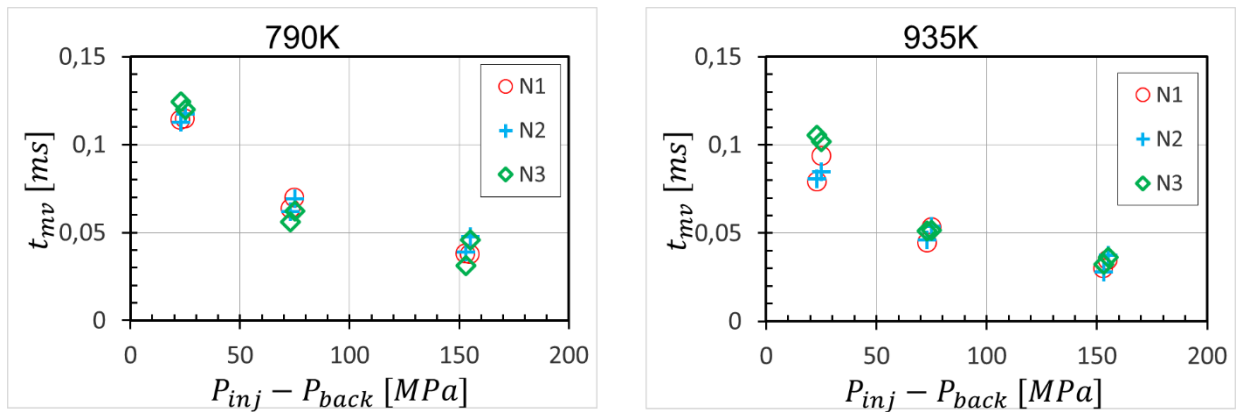$LL\ [mm]=2.9 \cdot 10^7 \cdot D_{eff}\ [mm] \cdot \rho_a\ [kg/m^3]^{-0.5} \cdot T[K]^{-1.64} \cdot \Delta P\ [MPa]^{-0.52}$

$$LL\ [mm]= \frac{1.254 \cdot (1/4)^{0.5} \cdot (\pi/4)^{0.5} \cdot D_{eff}\ [mm] \cdot (\rho_f/\rho_a\ [kg/m^3])^{0.5}}{C_{mv} \cdot \tan(\theta_m/2)}$$

Figure 11: Liquid length correlations

Figure 12: Time to mix and vaporize vs. pressure drop

$t\,[ms]=0,26 \cdot P_b[MPa]^{-0,89} \cdot exp(2510,9/T[K]) \cdot P_i\,[MPa]^{-0,138}$

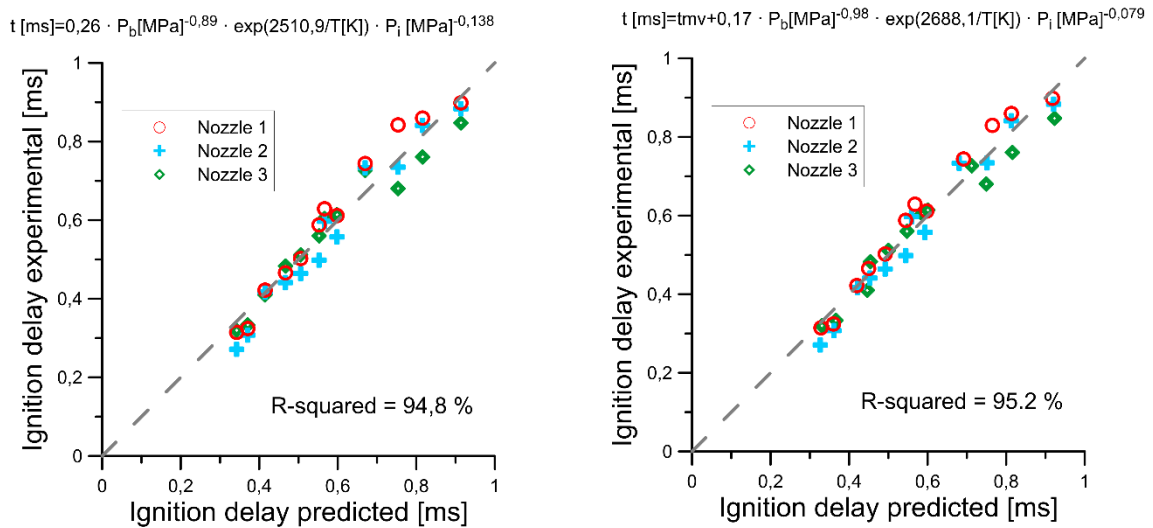$t\,[ms]=tmv+0,17 \cdot P_b[MPa]^{-0,98} \cdot exp(2688,1/T[K]) \cdot P_i\,[MPa]^{-0,079}$
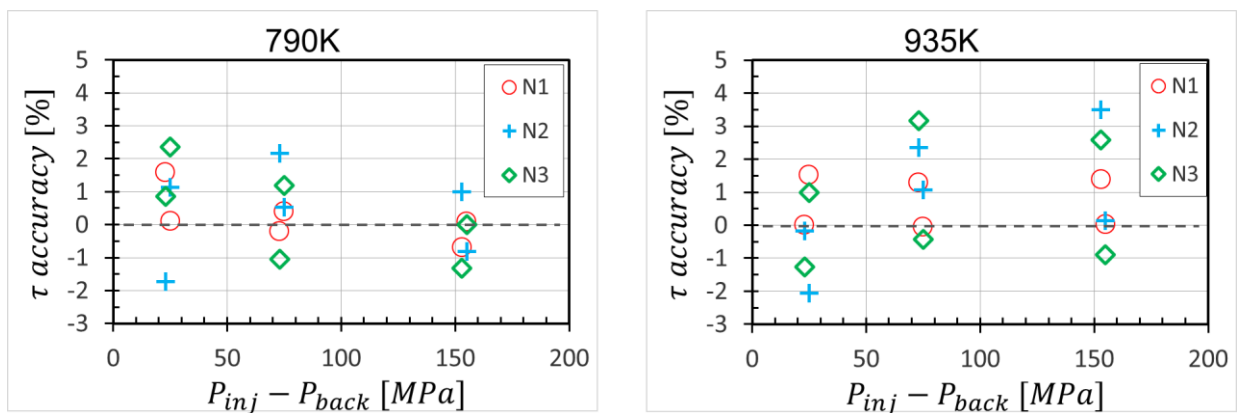

Figure 13: Ignition delay correlations

Figure 14: Improvement in the ignition delay correlation between the new (w/ t_{mv}) and

old (w/o t_{mv}) formulations